ADVANCED THEORY AND SIMULATIONS
www.advtheorysimul.com

Enhanced Terahertz Spectral-Fingerprint Detection of α-Lactose Using Sub-Micrometer-Gap On-Chip Waveguides

Sae June Park, Rowan S. Parker-Jervis, and John E. Cunningham**

We investigate using finite element methods how sub-micrometer to micrometer-scale coplanar waveguide (CPW) can be used for the detection of fingerprint spectra of very small (of order 10^{-14} mL) volumes of analytes in the terahertz (THz) frequency range. The electric field distribution is investigated near the waveguide for various gap widths between the center conductor and ground plane using a finite element simulation (ANSYS High Frequency Structure Simulator, HFSS). Taking lactose monohydrate as an exemplar material, a Drude–Lorentz model is combined for its real and imaginary permittivities with this numerical simulation, finding a significant enhancement in fingerprint detection as the gap width is reduced; the electric field in the CPW is found to increase by a factor ≈14 times moving from a 20 to 0.5-µm-wide gap between center conductor and ground plane, while the on-resonance THz absorption increases ≈14 times. The effective absorption coefficient of the lactose at 530 GHz is investigated as a function of the slot width for various lactose block thicknesses to understand how change in the field confinement and in the effective overlap between the lactose block and incident THz waves affect the effective absorption coefficient.

1. Introduction

A wide range of polycrystalline materials including lactose,[1] the common explosives RDX,[2] SX2,[2] and C–4,[3] as well as pharmaceutical drugs such as Alprazolam,[4] and Ibuprofen[4] exhibit spectral fingerprints in THz frequency range; and have been intensively investigated by free-space THz time-domain spectroscopy (THz-TDS) which is a non-contact, and nondestructive detection technique.[5,6] However, detecting spectral fingerprints of target materials with free-space THz-TDS can be challenging when the volume of the target material is small relative to the wavelength of the incident THz waves, owing to the small scattering cross-section between the THz waves and target material.[7] Plasmonic structures such as slot antennas[8] and photonic crystals[9] have been introduced to overcome this limitation. Often, α-lactose is used as a test material since it is relatively inert, nonpoisonous, and has narrow linewidth in its low-THz range resonances, while being readily available.[10,11] Previously, Park et al.[8] reported colossal absorption of 20 ng of lactose using a nanogapped slot antenna based on plasmonic sensors specifically designed to resonate at the resonant frequency of lactose while Cheng et al.[9] exploited a high-Q resonance in a photonic crystal cavity for sensitive detection of the lactose spectra. In both of these studies, plasmonic structures were predesigned to make them resonate at the target material's absorption frequency in order to detect the spectral fingerprint of the target material with enhanced sensitivity.

On the other hand, we previously showed that on-chip THz waveguides such as microstrip-line,[11] and Goubau-line[12] can also be used to recover the absorption spectra of polycrystalline materials in a broadband range (up to 2 THz) even without such resonant structures.[12] It is noteworthy that on-chip THz systems can record spectra from small sample volumes relative to those used in free-space THz-TDS spectroscopy systems.[13] It is therefore interesting to investigate methods based on on-chip THz waveguides that can further enhance their sensitivity for detecting spectra of materials.

CPW is a well-known high frequency transmission line consisting of a three-conductor structure comprising two ground planes separated by a gap on either side of a signal conductor[14,15] which has been widely adopted in on-chip THz systems. THz waves propagate along the slot gap with a well-confined electric field that can nonetheless interact with adjacent small systems such as 2D electron gas channels, for example.[14,15] We previously reported a giant magnetoresistance in a tapered sub-micrometer-gapped CPW structure formed from a magnetic multilayer.[16] The area of electric field confinement in the slot gap decreased as the CPW was tapered down to ≈0.5 µm, while the associated magnitude of the electric field increased.[16] It

S. J. Park
School of Electronic Engineering and Computer Science
Queen Mary University of London
London E1 4NS, UK
E-mail: s.j.park@qmul.ac.uk

S. J. Park, R. S. Parker-Jervis, J. E. Cunningham
School of Electronic and Electrical Engineering
University of Leeds
Leeds LS2 9JT, UK
E-mail: j.e.cunningham@leeds.ac.uk

The ORCID identification number(s) for the author(s) of this article can be found under https://doi.org/10.1002/adts.202100428

DOI: 10.1002/adts.202100428

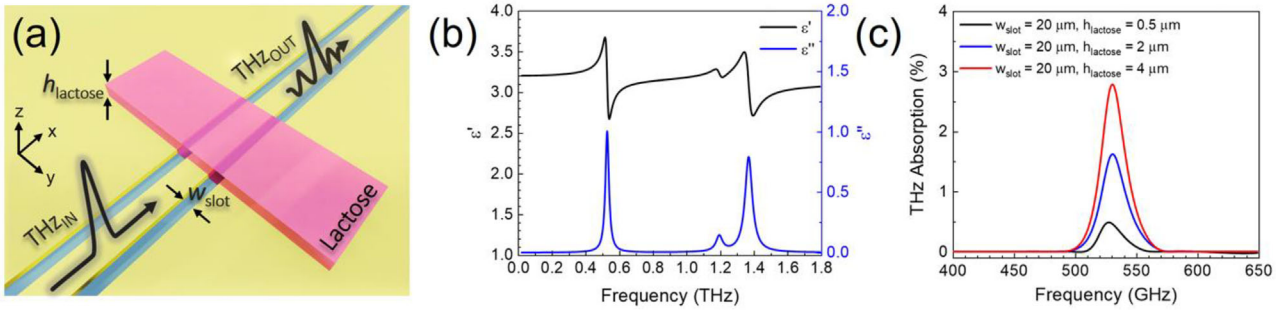

Figure 1. a) Schematic of the simulation model used. α-lactose block with the thickness of $h_{lactose}$ is located on the CPW with the slot with w_{slot}. b) Modelled real and imaginary permittivities of lactose in the THz frequency range. c) THz absorption of the CPW with w_{slot} = 20 μm for three different thickness of lactose, $h_{lactose}$ = 0.5, 2, and 4 μm.

is therefore interesting to investigate the potential for use of such waveguides for spectral absorption measurements of target materials.

Here, we provide a systematic study demonstrating the sensitivity of different CPW geometries for the direct THz fingerprint detection of polycrystalline materials without recourse to resonator structures. Specifically, a range of CPW slots gap widths were simulated to study both the electric field confinement of THz waves this produces, and the associated effect on the measured THz absorption that can be obtained from target materials.

2. Simulation Method

We used ANSYS high-frequency structure simulator (HFSS) to calculate the frequency-dependent transmission (S_{21}) of an α-lactose block located on CPW structures on a quartz substrate. **Figure 1**a shows a schematic of a CPW undergoing THz transmission coupled to a lactose block loaded the CPW from above and whose properties are directly sensed by the evanescent field in the waveguide. The center conductor of the CPW was defined with center conductor widths in the range of 750 nm – 30 μm, with a metal thickness of 150 nm,[14–16] a length of 150 μm, and was given slot gap widths (w_{slot}) in the range of 0.5–20 μm between the center conductor and the neighboring ground planes. An α-lactose block with a thickness of $h_{lactose}$, a width of 120 μm, and length of 50 μm was used as the exemplar target material.[10,11] The center of the α-lactose block was located at $x = 0$, $y = 0$, and $z = h_{lactose}/2$, using the coordinate system shown in Figure 1a. To obtain S_{21} of the CPW with a loaded lactose block for various w_{slot} and $h_{lactose}$, two-port S-parameter simulations were performed. The THz signals were generated from wave-ports directly coupled to the CPW. A radiation boundary condition was used in the model to remove any incident electric and magnetic fields on the boundaries of the simulation. Cross-sections of the electric field distribution at 530 GHz (corresponding to the lowest frequency absorption peak of lactose) were calculated at the middle of the CPW structure for various slot gap widths to investigate the electric field confinement dependence on w_{slot}. A permittivity of 3.8 was used for the quartz substrate, which is valid for the relevant frequency range (50–1100 GHz) in typical experiments.[17]

Table 1. Parameters used for modelling of the Drude–Lorentz dielectric function of lactose.

ϵ_∞	3.12		
Resonance and damping frequencies [THz]	$p = 1$	$p = 2$	$p = 3$
ω_p	0.53	1.20	1.37
γ_p	0.0253	0.0472	0.0521

Real and imaginary permittivities of lactose were modelled as shown in Figure 1b using the Drude–Lorentz dielectric function[18]

$$\varepsilon_r = \varepsilon_\infty + \sum_{p=1}^{3} \frac{{\omega_p}^2}{{\omega_p}^2 - \omega^2 - j\gamma_p\omega} \quad (1)$$

where ϵ_∞ is the off-resonance background permittivity of lactose, ω_p and γ_p are the angular frequency and damping rate of each absorption oscillation respectively. The parameters used are tabulated in **Table 1**.[1,18,19] The loss tangent was then calculated by dividing the imaginary permittivity by the real permittivity.[20] The frequency dependent permittivity and loss tangent were both used as data within HFSS in the simulation. We note that the absorption peaks of lactose are located at 0.53, 1.20, and 1.37 THz with full width at half maximums of 25, 6, and 52 GHz, respectively.[11,21]

3. Simulation Results and Discussion

To investigate the sensitivity of the THz CPW device for fingerprint detection of the α-lactose block, we begin with comparing the THz absorption of the CPW with w_{slot} of 20 μm for three different $h_{lactose}$, 0.5, 2, and 4 μm in Figure 1c. The THz absorption of the lactose block at 530 GHz was found to be 2.79%, 1.62%, and 0.46% for $h_{lactose}$ = 4, 2, 0.5 μm, respectively. The THz absorption strength at 530 GHz decreases as $h_{lactose}$ decreases since the interacting cross-sectional overlap between the lactose block and incident THz waves decreases as the lactose block thickness decreases.

To study the effect of w_{slot} on the electric field confinement and distribution, the amplitude of the electric field near the

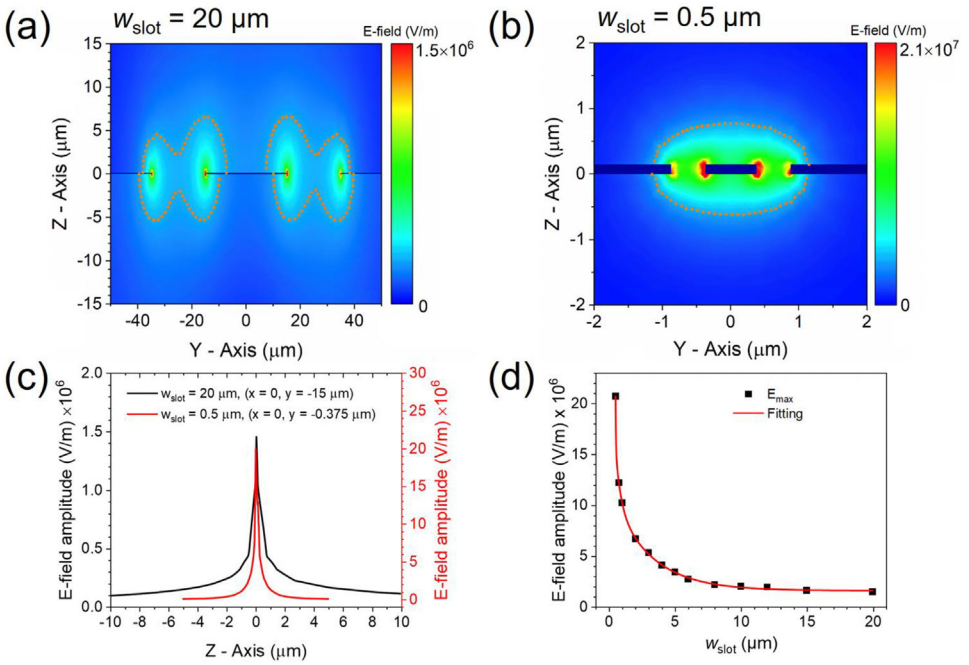

Figure 2. Field distribution near the CPW slot gap area (at $x = 0$) for a) $w_{slot} = 20$ μm and b) $w_{slot} = 0.5$ μm. Dotted orange lines show the field confinement area, as defined in the text. c) The electric field line profiles at edge of the center conductor along the z-axis, extracted from at $y = -15$ μm in a) (black line) and at $y = -0.375$ μm in (b) (red line). d) The amplitude of the maximum electric field near the CPW slot as a function of w_{slot}.

CPW structures were investigated at the absorption frequency of α-lactose (530 GHz) along the z–y plane (at $x = 0$) for both devices with w_{slot} of 20 and 0.5 μm in **Figure 2**a,b, respectively. The CPW device with $w_{slot} = 0.5$ μm shows highly confined electric field distribution compared to the device with $w_{slot} = 20$ μm. For simplicity, we define an area containing electric field strengths within one order of magnitude of the maximum electric field strength as the area of field confinement (see Figure 2a,b). The confinement areas of 478.4 and 2.3 μm^2 were thus obtained for the CPW devices with $w_{slot} = 20$, and 0.5 μm, respectively. In Figure 2c, we plotted the electric field amplitude as a function of the vertical position (z) at the edge of the center conductor at $x = 0$, $y = -15$ μm, and $x = 0$, $y = -0.375$ μm extracted from Figure 2a,b, respectively. We note that the electric field amplitude decays exponentially towards both the substrate and the air.[22] The decay lengths of the electric field amplitude obtained by an exponential fit in air ($z > 0$ μm) and substrate ($z < 0$ μm) decreased ≈3.6 times from 0.98 μm ($w_{slot} = 20$ μm) to 0.27 μm ($w_{slot} = 0.5$ μm) in the air, and ≈5.5 times from 1.31 μm ($w_{slot} = 20$ μm) to 0.24 μm ($w_{slot} = 0.5$ μm) in the substrate, respectively. In Figure 2d, we plot the maximum electric field amplitude near the edge of the CPW center conductor as a function of w_{slot} in the range 0.5–20 μm. The maximum amplitude of the field for the device with $w_{slot} = 0.5$ μm was increased ≈14 times compared to a device with $w_{slot} = 20$ μm (from 1.5×10^6 to 21×10^6 V m^{-1}, respectively). These results confirm that reducing w_{slot} in CPW is an effective way to increase the amplitude of confined THz field in the CPW slot.

The amplitude of the maximum electric field near the CPW slot as a function of w_{slot}.

In **Figure 3**, we investigate the effect of w_{slot} on the sensitivity for detecting spectral absorption of α-lactose for various w_{slot} and $h_{lactose}$ in the range of 0.5–20 μm, and 0.5–30 μm, respectively. Figure 3a shows the change of THz absorption of the α-lactose block with $h_{lactose} = 0.5$ μm located on the CPW devices for five different w_{slot} of 20, 10, 5, 1, and 0.5 μm. As w_{slot} decreases from 20 to 0.5 μm, while the absorption at 530 GHz significantly increases ≈14 times (from 0.46% to 6.58%) owing to the enhancement of the electric field amplitude in the CPW slot. In Figure 3b, we plot the THz absorption of the α-lactose block as a function of $h_{lactose}$ for various w_{slot} in the range of 0.5–20 μm. It is clear that THz absorption increases as $h_{lactose}$ increases and saturates at a specific $h_{lactose}$. It is also shown that the CPW device with narrower w_{slot} exhibits faster saturation behavior in THz absorption as $h_{lactose}$ increases owing to the highly confined and fast decaying electric field near the substrate–air interface as discussed in Figure 2.

In **Figure 4**, we estimate how sensitive our sub-micrometer-gapped ($w_{slot} = 0.5$ μm) CPW is by comparing the initial slope (sensitivity) of the THz absorption at 530 GHz – $h_{lactose}$ curve in the linear region ($h_{lactose} < 1$ μm) in Figure 3b. Figure 4a shows the sensitivity extracted from Figure 3b as a function of w_{slot}. As w_{slot} decreased from 20 to 0.5 μm, the sensitivity increased ≈14 times. It is noteworthy that THz waves propagating in each device with different w_{slot} interact with different volumes of α-lactose in the CPW field confinement area as shown in Figure 2a,b. We also note that presence of α-lactose in the CPW field confinement makes little difference to the overall field distribution. The volumes of α-lactose in the CPW field confinement area were estimated by calculating the overlap between the α-lactose block with a thickness of $h_{lactose}$, a width of 120 μm, and length of 50 μm and the field confinement areas shown in Figure 2a,b. For example, the device with $w_{slot} = 20$ μm contains 1.33×10^{-12} mL of α-lactose in the confinement area when $h_{lactose} = 0.5$ μm, whereas the de-

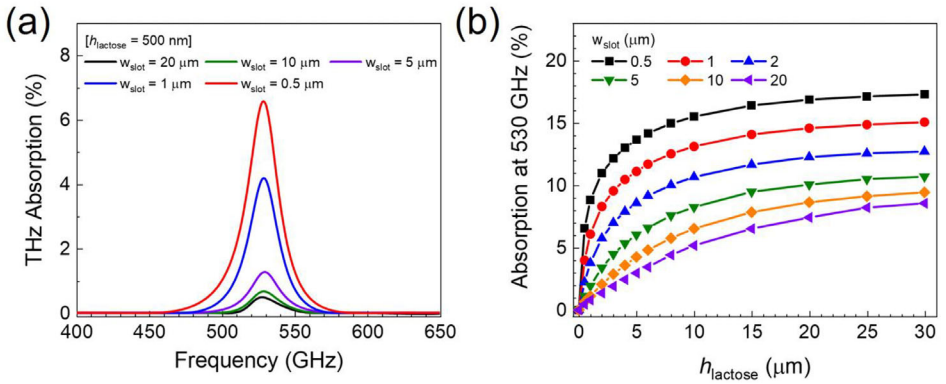

Figure 3. a) THz absorption of the CPW with 0.5-μm-thick lactose block for five different gaps between the center conductor and ground planes w_{slot}: 0.5, 1, 5, 10, and 20 μm. b) THz absorption at 530 GHz as a function of $h_{lactose}$ for various w_{slot}.

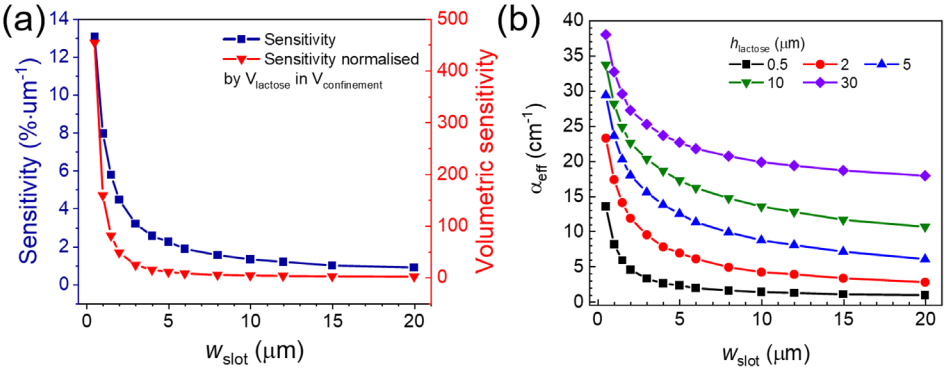

Figure 4. a) Sensitivity defined by the initial slope of the THz absorption – $h_{lactose}$ curve and volumetric sensitivity enhancement factor as a function of w_{slot}. b) Effective absorption coefficient (α_{eff}) as a function of w_{slot} for various $h_{lactose}$.

vice with $w_{slot} = 0.5$ μm contains 4.41×10^{-14} mL of α-lactose. The volumetric sensitivity enhancement factor can also be calculated by dividing the sensitivity by the volume of α-lactose in the CPW field confinement area at each w_{slot}, considering the lateral extent of the block along the CPW and the interacting cross-section; this is also presented in Figure 4a. The volumetric sensitivity enhancement factor yielded a 453-fold increase for $w_{slot} = 0.5$ μm compared to $w_{slot} = 20$ μm. To quantify the effective absorption coefficient (α_{eff}) of the lactose resonance at 530 GHz, we calculated α_{eff} as a function of w_{slot} for various $h_{lactose}$ in Figure 4b using $\alpha_{eff} = -(1/t)\ln(T/T_0)$. T and T_0 are the transmissions with and without the lactose block, and t is the length of the lactose block. Here, α_{eff} is proportional to the absorption cross-section σ, while σ is proportional to the electric field intensity ($\alpha_{eff} \propto \sigma \propto E^2$).[8] As w_{slot} decreases, an increase in the electric field confinement induces an increase in the absorption cross-section, resulting in an enhancement in α_{eff}, while decreasing $h_{lactose}$ induced a decrease in α_{eff} as it reduces the effective cross-section between the propagating THz wave and the lactose block. We note that α_{eff} of 37.98 cm^{-1} was obtained for $w_{slot} = 0.5$ μm, $h_{lactose} = 30$ μm.

4. Conclusion

We suggest a novel method for the enhanced detection of the fingerprint of target material in the THz frequency range using sub-micrometer-gapped CPW structures. α-lactose was chosen as an example target material and permittivities of α-lactose were modelled using the Drude–Lorentz function. Electric field distribution and its confinement near the CPW show that reducing the slot width of the CPW effectively enhances the electric field confined in the CPW slot. We also showed that THz absorption of α-lactose at 530 GHz can be enhanced up to ≈14 times by reducing the CPW slot width from 20 to 0.5 μm. The enhancement factor obtained by normalizing the sensitivity to the actual volume of lactose interacting with propagating THz waves was extracted as a function of w_{slot} and yielded ≈453 for $w_{slot} = 0.5$ μm. We note that this approach for detecting absorption spectra of a small amount of analyte across a broadband THz frequency range can overcome the severe limitation of existing methods based on plasmonic structures that need to be designed to resonate at absorption peaks of target materials to achieve the field enhancement, thereby limiting their applicability to the detection of unknown target materials.

Acknowledgements

The authors gratefully acknowledge funding from Engineering and Physical Sciences Research Council (EPSRC), grant numbers EP/R00501X/1, EP/P021859/1, EP/V004743/, and EP/V047914/1, and from the UK National Physical Laboratory; The data associated with this paper is available from the University of Leeds at https://doi.org/10.5518/1054.[23]

Conflict of Interest

The authors declare no conflict of interest.

Data Availability Statement

The data associated with this paper is available from the University of Leeds at https://doi.org/10.5518/1054.

Keywords

fingerprint detection, on-chip waveguide, sensitivity enhancement, terahertz sensors

Received: October 1, 2021
Revised: November 11, 2021
Published online:

[1] K. Moon, Y. Do, H. Park, J. Kim, H. Kang, G. Lee, J. H. Lim, J. W. Kim, H. Han, *Sci. Rep.* **2019**, *9*, 16915.
[2] A. G. Davies, A. D. Burnett, W. Fan, E. H. Linfield, J. E. Cunningham, *Mater. Today* **2008**, *11*, 18.
[3] K. Yamamoto, M. Yamaguchi, F. Miyamaru, M. Tani, M. Hangyo, T. Ikeda, A. Matsushita, K. Koide, M. Tatsuno, Y. Minami, *Jpn. J. Appl. Phys.* **2004**, *43*, L414.
[4] M. Karaliunas, R. Venckevišius, I. Kašalynas, U. Puc, A. Abina, A. Jeglič, A. Zidanšek, G. Valušis, presented at Proc. SPIE – Int. Soc. Opt. Eng., San Diego, California, United States, 31 August **2015**.
[5] S. S. Dhillon, M. S. Vitiello, E. H. Linfield, A. G. Davies, M. C. Hoffmann, J. Booske, C. Paoloni, M. Gensch, P. Weightman, G. P. Williams, E. Castro-Camus, D. R. S. Cumming, F. Simoens, I. Escorcia-Carranza, J. Grant, S. Lucyszyn, M. Kuwata-Gonokami, K. Konishi, M. Koch, C. A. Schmuttenmaer, T. L. Cocker, R. Huber, A. G. Markelz, Z. D. Taylor, V. P. Wallace, J. Axel Zeitler, J. Sibik, T. M. Korter, B. Ellison, S. Rea, P. Goldsmith, et al., *J. Phys. D: Appl. Phys.* **2017**, *50*, 043001.
[6] D. M. Mittleman, *J. Appl. Phys.* **2017**, *122*, 230901.
[7] S. J. Park, J. T. Hong, S. J. Choi, H. S. Kim, W. K. Park, S. T. Han, J. Y. Park, S. Lee, D. S. Kim, Y. H. Ahn, *Sci. Rep.* **2014**, *4*, 4988.
[8] H. R. Park, K. J. Ahn, S. Han, Y. M. Bahk, N. Park, D. S. Kim, *Nano Lett.* **2013**, *13*, 1782.
[9] W. Cheng, Z. Han, Y. Du, J. Qin, *Opt. Express* **2019**, *27*, 16071.
[10] H. Amarloo, S. Safavi-Naeini, *Opt. Express* **2021**, *29*, 17343.
[11] M. B. Byrne, J. Cunningham, K. Tych, A. D. Burnett, M. R. Stringer, C. D. Wood, L. Dazhang, M. Lachab, E. H. Linfield, A. G. Davies, *Appl. Phys. Lett.* **2008**, *93*, 182904.
[12] C. Russell, C. D. Wood, A. D. Burnett, L. Li, E. H. Linfield, A. G. Davies, J. E. Cunningham, *Lab Chip* **2013**, *13*, 4065.
[13] S. J. Park, J. Cunningham, *Sensors* **2020**, *20*, 4264.
[14] S. J. Park, S. Zonetti, R. S. Parker-Jervis, J. Wu, C. D. Wood, L. H. Li, A. G. Davies, E. H. Linfield, O. Sydoruk, J. E. Cunningham, *Opt. Express* **2021**, *29*, 12958.
[15] J. Wu, A. S. Mayorov, C. D. Wood, D. Mistry, L. Li, W. Muchenje, M. C. Rosamond, L. Chen, E. H. Linfield, A. G. Davies, J. E. Cunningham, *Sci. Rep.* **2015**, *5*, 15420.
[16] N. Peters, M. Rosamond, L. Li, E. H. Linfield, A. G. Davies, M. Ali, B. J. Hickey, J. Cunningham, *Appl. Phys. Lett.* **2018**, *112*, 181103.
[17] H. Lamela, E. Dadrasnia, D. M. Lee, S. Baik, M. B. Kuppam, F. Garet, J. L. Coutaz, presented at Proc. SPIE, San Diego, California, United States, 27 September **2012**.
[18] X. Shi, Z. Han, *Sci. Rep.* **2017**, *7*, 13147.
[19] A. Roggenbuck, H. Schmitz, A. Deninger, I. C. Cámara Mayorga, J. Hemberger, R. Güsten, M. Grüninger, *New J. Phys.* **2010**, *12*, 043017.
[20] K. Manjunatha, V. Jagadeesha Angadi, K. M. Srinivasamurthy, S. Matteppanavar, V. K. Pattar, U. Mahaboob Pasha, *J. Supercond. Novel Magn.* **2020**, *33*, 1747.
[21] E. R. Brown, J. E. Bjarnason, A. M. Fedor, T. M. Korter, *Appl. Phys. Lett.* **2007**, *90*, 061908.
[22] S. J. Park, J. Cunningham, *Sensors* **2020**, *20*, 3133.
[23] S. J. Park, R. J. Parker-Jervis, J. E. Cunningham, *Dataset associated with "Enhanced Terahertz Spectral-Fingerprint Detection of α-Lactose Using Sub-Micron-Gap On-Chip Waveguides"*, **2021**. The data associated with this paper is available from the University of Leeds at https://doi.org/10.5518/1054.